The Astrophysical Journal, 625:L67–L70, 2005 May 20

BROADBAND METRIC-RANGE RADIO EMISSION ASSOCIATED WITH A MORETON/EIT WAVE

B. Vršnak,[1] J. Magdalenić,[1] M. Temmer,[2] A. Veronig,[2] A. Warmuth,[3] G. Mann,[3] H. Aurass,[3] and W. Otruba[4]
Received 2005 March 15; accepted 2005 April 6; published 2005 April 21

ABSTRACT

We present the evolution and kinematics of a broadband radio source that propagated collaterally with an Hα/EIT wave, linking it with the type II burst that was excited higher up in the corona. The NRH wave emission extended from the frequency $f \approx 327$ to $f < 151$ MHz and was considerably weaker than the flare-related type IV burst. The emission centroid propagated at a height of 0–200 Mm above the solar limb and was intensified when the disturbance passed over enhanced coronal structures. We put forward the ad hoc hypothesis that the NRH wave signature is optically thin gyrosynchrotron emission excited by the passage of the coronal MHD fast-mode shock. The identification of radio emission associated with the coronal wave front is important since it offers us new diagnostic information that could provide us with better insight into the physical conditions in the disturbance itself.

Subject headings: shock waves — Sun: corona

1. INTRODUCTION

Eruptive releases of free energy stored in the solar corona, manifesting as coronal mass ejections (CMEs) and flares, under certain circumstances cause spectacular wavelike disturbances that traverse large distances of the solar atmosphere. The longest known signatures of these disturbances are type II radio bursts (Wild & McCready 1950) and chromospheric Moreton waves (Moreton & Ramsey 1960). Both phenomena propagate at velocities in the order of 1000 km s^{-1} and are very tightly related, indicating a common nature of the underlying disturbance (e.g., Harvey et al. 1974; Uchida 1974; Klassen et al. 2000; Khan & Aurass 2002). The close association of the two phenomena was explained by Uchida (1968, 1974), who put forward the sweeping-skirt hypothesis, according to which Moreton waves are just "surface tracks" of the coronal fast-mode MHD shocks that excite type II bursts higher up in the corona.

Although an EUV counterpart of the Moreton wave was already reported by Neupert (1989), a new era of investigation of coronal waves effectively begun after direct imaging of disturbances by the Extreme-ultraviolet Imaging Telescope (EIT) on the *Solar and Heliospheric Observatory* (*SOHO*). The discovery of "EIT waves" (Thompson et al. 1998) prompted the search for wave signatures in other spectral domains. Soon thereafter, Moreton-like disturbances were revealed in soft X-rays (Narukage et al. 2002; Khan & Aurass 2002; Hudson et al. 2003; Warmuth et al. 2005), He I λ10830 (Gilbert et al. 2001; Vršnak et al. 2002; Gilbert & Holzer 2004), microwaves (Warmuth et al. 2004; White & Thompson 2005), etc. (for an overview and historical background see, e.g., Zhukov & Auchère 2004, Vršnak 2005, and Warmuth 2005).

In this Letter we present the discovery of an additional signature of coronal waves: a broadband weak coronal radio emission associated with the Moreton wave that was launched by the flare/CME event that took place around 10 UT on 2003 November 3. Herein, we focus primarily on the morphology and kinematics of the newly discovered feature, and its relationship with the Hα/EUV disturbance. The question as to whether the wave in the considered event was ignited by the flare or was driven by the CME will be addressed in a separate paper (B. Vršnak et al. 2005, in preparation) since it requires a very detailed analysis of the evolution of the CME and the flare, which is beyond the scope of this Letter.

2. THE DATA

The Hα Moreton wave is traced utilizing Kanzelhöhe Solar Observatory (KSO) Hα filtergrams (Otruba & Pötzi 2003). KSO routinely takes full-disk Hα images with a time cadence of ~5 s and a spatial resolution of 2″.2 $pixel^{-1}$. When the flare mode is triggered, images in the blue and red wing of the Hα spectral line (at the off-band center wavelength of Hα − 0.3 Å and Hα + 0.4 Å) are taken with a cadence of about 1 image per minute in each wing.

The propagation of the EIT wave is measured in the Fe XII 195 Å images gained by EIT (Delaboudiniere et al. 1995). These images show coronal structures at temperatures around 1.5 MK. The EIT images have a resolution of 2″.6 $pixel^{-1}$ and a field of view of 1.4 solar radii.

Positions of radio sources at 432, 411, 327, 237, 164, and 151 MHz are measured employing data recorded by the Nançay Multifrequency Radioheliograph (NRH; Kerdraon & Delouis 1997). NRH provides 8 images per second at each frequency with the beam size of a few arcminutes at the lowest two frequencies and around 1′ at 327 MHz.[5]

The evolution of dominant NRH sources was compared with the corresponding features in the dynamic spectrum of the Potsdam-Tremsdorf Radiospectrograph, covering the range 40–800 MHz with a time resolution of 0.1 s (Mann et al. 1992).

3. MORPHOLOGY AND BEHAVIOR

The two-ribbon X3.9 flare of 2003 November 3 was centered at N8°, W77°, at the northern edge of NOAA AR 10488 (Fig. 1). The *GOES* 1–8 Å burst started around 09:43 UT and

[1] Hvar Observatory, Faculty of Geodesy, Kačićeva 26, HR-10000 Zagreb, Croatia.
[2] Institute of Physics, University of Graz, Universitätsplatz 5, A-8010 Graz, Austria.
[3] Astrophysikalisches Institut Potsdam, An der Sternwarte 16, 14482 Potsdam, Germany.
[4] Kanzelhöhe Solar Observatory, Institute of Physics, University of Graz, A-9521 Treffen, Austria.

[5] For details see http://bass2000.obspm.fr.

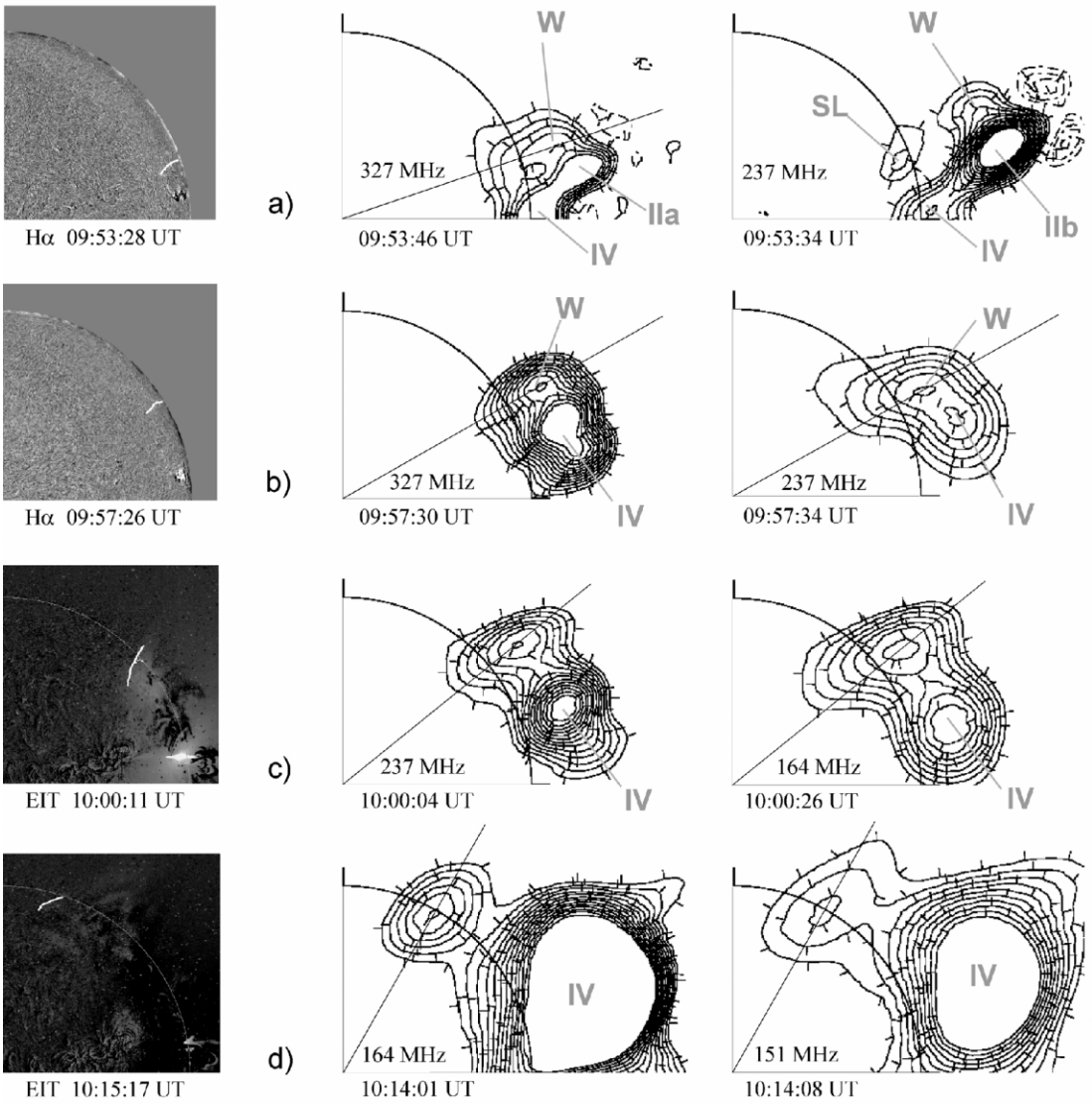

FIG. 1.—*Left column*: Moreton wave seen in KSO-Hα difference images (panels *a* and *b*) and EIT difference images (panels *c* and *d*). Wave fronts are marked by white lines. *Middle and right columns*: Propagation of the associated NRH wave source (marked by W). The type II and IV burst sources are indicated, as well as the sidelobe (SL) image of the type II burst in the uppermost right panel. In each heliogram the line defining the position angle of the NRH wave centroid is drawn.

attained a double maximum at 09:54/10:02 UT. Detailed descriptions of the flare morphology and the energy release evolution based on the X-ray observations are presented by Liu et al. (2004) and Veronig et al. (2005), whereas Dauphin et al. (2005) analyzed the flare-associated type IV radio emission. The flare occurred in conjunction with a fast CME ($v \approx 1400$ km s^{-1}), heading along the position angle P.A. $\approx 300°$. The back extrapolation of the CME trajectory indicates that it was launched between 09:40 and 09:55 UT.

The Moreton wave propagated closely by the solar limb, in the northward direction from the flare site (Fig. 1). The first Hα wave front was measured at 09:53:28 UT, at the position angle P.A. $\approx 289°$, i.e., some $d \approx 120$ Mm from the flare center. The last Hα wave front was measured at 10:00:30 UT at P.A. $\approx 312°$ ($d \approx 400$ Mm). After that, the Hα disturbance became too weak to be measured. In the first EIT image showing the wave (10:00 UT), the EUV wave front was cospatial with the last measured Hα wave front. The wave is also visible in the next EIT image (10:15 UT), at the location P.A. $\approx$ 340°–350° ($d \approx 750$ Mm). Both EIT images reveal the coronal disturbance also above the limb (Figs. 1*c* and 1*d*).

The dominant features in the NRH intensity maps were several flare-associated type IV burst sources (Dauphin et al. 2005) and two strong type II burst sources (Fig. 1*a*). However, in the period 09:54–10:15 UT the radioheliograms also reveal a weak radio source above the northwest limb (Fig. 1), moving synchronously with the Hα/EIT wave (hereafter the "NRH wave"). The source was characterized by a broadband emission recorded at all NRH frequencies $f \leq 327$ MHz, with the emission centroid located at a height varying between 0 and 200 Mm. The NRH wave source was weaker than the type II burst sources by a factor of 10 at 151 and 164 MHz, 10–100 at 237 MHz, and almost 100–1000 at 327 MHz. The type II burst sources were stronger at higher frequencies, whereas the NRH wave was brighter at lower frequencies. The intensity of the NRH wave was gradually weakening in time/distance: at 327 and 237 MHz it decreased by a factor of 10, and at 164 and 151 by a factor of 2.

At 164 and 151 MHz, the NRH wave sources could be identified only beyond ΔP.A. $\approx 30°$ from the flare site (Figs. 1 and 2)—at smaller distances the emission was merged with the

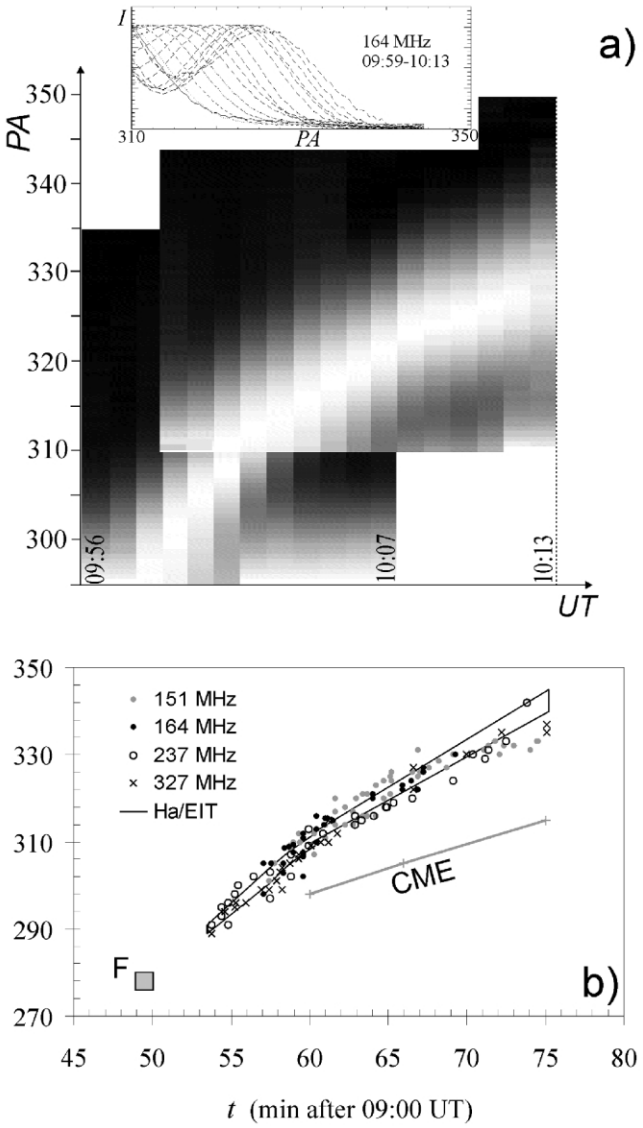

FIG. 2.—(*a*) 164 MHz NRH wave P.A.(*t*) stack plot, superposed on the 237 MHz stack plot (for details see the main text). In the inset at the top we show the relative intensities *I*(P.A.) for all 164 MHz stacks. (*b*) Position angles P.A.(*t*) of the measured NRH wave centroids compared with the Hα/EIT wave (black lines). The large gray square (F) marks the position of the flare in the P.A.(*t*) space at the time of the hard X-ray impulsive peak, whereas the gray line depicts the northward expansion of the CME.

flare type IV and/or type II burst sources due to insufficient spatial resolution. (However, even before the sources split, an emission "bulge" can be seen at the northern edge of the type IV source.) At 327 and 237 MHz, the NRH wave sources are distinguishable from the type II and IV sources closer to the flare site than they are at lower frequencies (Figs. 1 and 2). On the other hand, because of the lower intensity it is more difficult to identify them at large distances.

In Figure 1 we present the heliograms in which the centroid of the NRH wave source could be unambiguously identified, and they are closest in time to the Hα/EIT wave images. The number and distribution of intensity contours are chosen in such manner as to show the NRH wave centroid as clearly as possible. Besides the NRH wave (W) we mark the type IV burst source (IV) and the two type II burst sources (IIa and IIb) that are identified in the dynamic spectrum as two independent lanes of different drift rates. The 327 MHz heliogram shown in Figure 1*a* reveals an emission pattern that connects the type II burst source (IIa) with the location of the Moreton wave. The heliograms presented in Figures 1*b*–1*d* clearly illustrate that the NRH wave was characterized by a broadband emission.

The horizontal extension of the NRH wave radio feature approximately corresponds to the beam size, whereas the vertical extension is generally larger than the beam width. This indicates that the radio emission comes from a relatively narrow, vertically elongated source. It becomes remarkably stretched in the vertical direction (almost over 1 solar radius) at the time when the perturbation reached the position angle of the coronal streamer located at P.A. $\approx 310°$.

The NRH wave was brightest when passing enhanced coronal structures at P.A. $\approx 285°$–$300°$ and $320°$–$330°$. At these locations the radio emission becomes prolonged, indicating that a local energy release was triggered by the disturbance.

4. KINEMATICS

The kinematics of the coronal wave is depicted in Figure 2. In Figure 2*a* we present two stack plots (237 and 164 MHz) showing the continuity of the NRH wave motion along the position angle direction. Each stack is obtained by sampling the intensity along the limb within the radial distance range $R = 1.05$–1.55. The 237 MHz stacks cover the range P.A. $= 295°$–$335°$ in the period 09:55–10:07 UT, whereas the 164 MHz stack plot spans from P.A. $= 310°$ to $350°$ in the interval 09:58–10:13 UT. The used radioheliograms are separated by approximately 1 minute (average deviation ± 5 s). Each stack is individually scaled to the maximum intensity in the considered P.A. range. The horizontal bright stripe at the bottom of the 237 MHz stack plot is the emission from the type IV burst source.

In order to compare the motion of the Hα/EIT wave and the NRH wave, we measured the position angle P.A. of both phenomena. We stress that due to the limited resolution, it is impossible to define the leading edge of the NRH wave perturbation; i.e., we cannot specify the "wave front" as in the case of the Hα/EIT wave.

Consequently, we are constrained to measure the position angle of the radio source centroid in the intensity contour maps (Fig. 1). It should be noted that we omitted measurements in all situations where the sidelobe images of either the type IV or the type II burst might affect the location of the NRH wave centroid.

In Figure 2*b* we compare the P.A.(*t*) dependence of the Moreton wave observed in Hα and in Fe XII 195 Å with the P.A.(*t*) dependence of the associated NRH wave. The error of the position measurements themselves are considerably smaller than the scatter of the data in Figure 2*b*. The graph clearly shows that both phenomena, i.e., the Hα/EIT wave and the NRH wave, follow the same kinematical curve. In the graph we also show the P.A. of the flare (for the time of the impulsive peak of hard X-ray burst ≈09:49–09:50 UT), the expansion of the northward edge of the CME estimated from the coronal dimming in EIT images, and the appearance of the CME in the *SOHO* Large Angle and Spectrometric Coronagraph at 10:06 UT.

The quadratic fit through the P.A.(*t*) data shows a continuous deceleration of the Hα/EIT wave as well as of the NRH wave. If transformed to distances along the solar limb ($R = 1$), we find for the Hα/EIT wave a deceleration of $a = -310 \pm 50$ m s^{-2}, and for the NRH wave $a = -350 \pm 50$ m s^{-2}. At the time of the first measurable Hα/EIT wave front (09:53:28 UT) one finds a velocity of 660 km s^{-1}, whereas in the case of the

NRH wave the velocity is 650 km s^{-1}. At 10:15 UT the velocities drop to 270 and 180 km s^{-1}, respectively.

5. DISCUSSION AND CONCLUSION

The NRH wave feature propagated collaterally with the Hα/EIT wave and was associated with the coronal shock that caused a type II burst higher up in the corona. It was characterized by a relatively weak broadband emission, extending from ≈327 to below 151 MHz. The emission was stronger at higher frequencies, which is indicative of optically thin gyrosynchrotron emission (Dulk & Marsh 1982). Adopting the interpretation of the coronal disturbance in terms of the fast-mode MHD shock (Uchida 1974), and bearing in mind that at the shock the magnetic field is enhanced and the energy and density of electrons are increased, an enhancement of the gyrosynchrotron emissivity (Dulk & Marsh 1982) in the region behind the shock could indeed be expected. Note that White & Thompson (2005) interpreted the 17 GHz signature of the EIT wave observed on 1997 September 24 as an optically thin thermal bremsstrahlung from the plasma swept up by the wave.

Since the identification of radio emission associated with the coronal wave front offers us new diagnostic information (e.g., Aschwanden 2004), complementary to that provided by soft X-rays (see, e.g., Narukage et al. 2002 and Hudson et al. 2003), we hope that our finding will enable us to better comprehend the physical conditions in the coronal disturbance itself. Finally, the importance of finding an NRH wave signature is that it provides us with the possibility of tracing the disturbance at the highest cadence across a large distance range.

We are grateful to the NRH and *SOHO*/EIT teams for operating the instruments and performing the basic data reduction, as well as for their open data policy. We gratefully acknowledge financial support from the Austrian Science Fund (FWF project P15344). The work of A. W. was supported by DLR under grant 50 QL 0001. The stay of B. V. and J. M. at AIP was financed by DFG 436 KRO 113/8/0-1.

REFERENCES

Aschwanden, M. J. 2004, Physics of the Solar Corona (New York: Springer), chap. 15
Dauphin, C., Vilmer, N., Lüthi, T., Trottet, G., Krucker, S., & Magun, A. 2005, Adv. Space Res., submitted
Delaboudiniere, J.-P., et al. 1995, Sol. Phys., 162, 291
Dulk, G. A., & Marsh, K. A. 1982, ApJ, 259, 350
Gilbert, H. R., & Holzer, T. E. 2004, ApJ, 610, 572
Gilbert, H. R. Thompson, B. J., Holzer, T. E., & Burkepile, J.T. 2001, AGU Fall Meeting 2001, abstract SH12B-0746
Harvey, K. L., Martin, S. F., & Riddle, A. C. 1974, Sol. Phys., 36, 151
Hudson, H. S., Khan, J. I., Lemen, J. R., Nitta, N. V., & Uchida, Y. 2003, Sol. Phys., 212, 121
Kerdraon, A., & Delouis, J. 1997, in Coronal Physics from Radio and Space Observations, ed. G. Trottet (Heidelberg: Springer), 192
Khan, J. I., & Aurass, H. 2002, A&A, 383, 1018
Klassen, A., Aurass, H., Mann, G., & Thompson, B. J. 2000, A&AS, 141, 357
Liu, W., Jiang, Y. W., Liu, S., & Petrosian, V. 2004, ApJ, 611, L53
Mann, G., Aurass, H., Voigt, W., & Paschke, J. 1992, in Proc. First *SOHO* Workshop: Coronal Streamers, Coronal Loops, and Coronal and Solar Wind Composition (ESA SP-348; Paris: ESA), 129
Moreton, G. E., & Ramsey, H. E. 1960, PASP, 72, 357
Narukage, N., Hudson, H. S., Morimoto, T., Akiyama, S., Kitai, R., Kurokawa, H., & Shibata, K. 2002, ApJ, 572, L109
Neupert, W. M. 1989, ApJ, 344, 504
Otruba, W., & Pötzi, W. 2003, Hvar Obs. Bull., 27, 189
Thompson, B. J., Plunkett, S. P., Gurman, J. B., Newmark, J. S., St. Cyr, O. C., & Michels, D. J. 1998, Geophys. Res. Lett., 25, 2465
Uchida, Y. 1968, Sol. Phys., 4, 30
———. 1974, Sol. Phys., 39, 431
Veronig, A., et al. 2005, A&A, submitted
Vršnak, B. 2005, Eos, 86, 112
Vršnak, B., Warmuth, A., Brajša, R., & Hanslmeier, A. 2002, A&A, 394, 299
Warmuth, A. 2005, in Lecture Notes in Physics, in press
Warmuth, A., Mann, G., & Aurass, H. 2005, ApJ, submitted
Warmuth, A., Vršnak, B., Magdalenić, J., Hanslmeier, A., & Otruba, W. 2004, A&A, 418, 1101
White, S. M., & Thompson, B. 2005, ApJ, 620, L63
Wild, J. P., & McCready, L. L. 1950, Australian J. Phys., 3, 387
Zhukov, A. N., & Auchère, F. 2004, A&A, 427, 705